Geophys. J. Int. (0000) **000**, 1–7

Numerical Simulation of Magma Pathways and Vent Distribution in Rifts From the Early Stages to Maturity

Gaetano Ferrante[1,2], Eleonora Rivalta[1,3], Francesco Maccaferri[4]

[1] *Department of Physics and Astronomy, Alma Mater Studiorum, University of Bologna, Via Zamboni, 33, 40126 Bologna BO, Italy*
[2] *Department of Earth, Environmental and Planetary Sciences, Rice University, 6100 Main Street, Houston, TX 77005, USA. E-mail: gf15@rice.edu*
[3] *GFZ German Research Centre for Geosciences, Telegrafenberg, 14473 Potsdam, Germany*
[4] *National Institute of Geophysics and Volcanology (INGV), Osservatorio Vesuviano, Napoli 80124, Italy*

10 October 2022

SUMMARY
Volcanism in continental rifts is generally observed to shift over time from the inside of the basin to its flanks and conversely, but the controls on these switches are still unclear. Here we use numerical simulations of dike propagation to test the hypothesis that the spatio-temporal evolution of rift volcanism is controlled by the crustal stresses produced during the development of the rift basin. We find that the progressive deepening of a rift is accompanied by a developing stress barrier under the basin, which deflects ascending dikes, causing an early shift of volcanism from the inside to the flanks. The intensification of the barrier due to further deepening of the basin promotes the formation of lower crustal sill-like structures that can stack under the rift, shallowing the depth of magma injection, eventually causing a late stage of in-rift axial volcanism.

Key words: Continental tectonics: extensional, Magma migration and fragmentation, Pluton emplacement

1 INTRODUCTION

Continental rifting is the process by which the lithosphere is thinned in response to extensional forces of different origin that result in the formation of large scale fault-bounded basins (Condie 2013). Continental rifting is often accompanied by volcanism, which may be scarce or completely absent in melt-poor rifts or abundant in melt-rich rifts (Williams 1982; White 1992; Acocella 2021). Melt production may be caused by the rise of a mantle plume, asthenospheric upwelling in response to lithospheric stretching, or a combination of the two (Bott 2006; Acocella 2021), with the relative contributions of these processes in specific regions often debated (e.g. Fitton 1983; Lesne et al. 1998; Ivanov et al. 2015). How the mechanisms underlying the creation of the rift are linked to location and timing of volcanism and to melt abundance is still poorly understood.

Volcanism in rifts migrates over time and is often observed to follow some patterns that accompany the development of the rift basin. The formation of the rift excavation is usually preceded by a period of scattered volcanism, either associated with ground subsidence or uplift (e.g. Michon & Merle 2001; Corti 2009). After the formation of a rift basin, deformation is mainly accommodated by displacement on large boundary faults (e.g. Corti 2012). Volcanism, in turn, localizes in a more confined area through the formation of scattered vents, usually comprising the basin and part of the rift flanks (e.g. Logatchev & Florensov 1978; Michon & Merle 2001; Corti 2009). Developed basins are associated with large volcanic edifices on the flanks of the basin (e.g. Michon & Merle 2001), often called off-rift volcanoes, and stacked sills and underplated intrusions in the lower crust (Thybo & Nielsen 2009; Thybo & Artemieva 2013). Lastly, in mature rifts, volcanism focuses within the axial part of the rift, marking the onset of oceanic spreading (e.g. Kiselev 1987; Morton et al. 1979; Corti 2009). These patterns are commonly observed regardless the underlying cause of rifting, whether it is active or passive; this suggests a different common control. A comprehensive model of rift magmatism needs to explain, on the basis of a mechanically sound hypothesis, a number of observations: 1) the shifts in the location of eruptive vents at the earth's surface, 2) the failed eruptions of large magma volumes, which are instead accommodated as igneous intrusions according to specific emplacement patterns, 3) why the shifts from pattern to pattern occur rather abruptly, marking well-defined 'epochs' of volcanism, 4) the fact that different spatial patterns are often associated to discrete shifts in magma composition.

While no model so far has achieved such an overarching explanation of the spatio-temporal and geochemical patterns described above, there have been attempts to explain some of the observed shifts, with many authors focusing on the counterintuitive locations of off-rift volcanoes. Some studies attributed the occurrence of flank volcanism to the interaction of magma with boundary faults (e.g. Bosworth 1987; Corti et al. 2004). Bosworth (1987) ascribed the existence of off-rift volcanoes to the presence of low-angle detachment faults beneath asymmetric rifts, that would tap the asthenosphere and weaken the crust, facilitating magma migration far from the basin. Corti et al. (2004) developed centrifuge

models to propose that surface deformation controls the migration of magma towards the footwall of the boundary faults, that would in turn channel magma to the surface to feed off-axis volcanoes. However, these interpretations are not fully supported by independent observations for a number of reasons: in particular, there is little to no evidence of deeply penetrating detachment faults underlying extensional areas (Bott 2006; Ellis & King 1991) and propagation of magma through faults is now considered to be a minor mechanism (Pollard 1987; Ziv et al. 2000). Indeed, it is now increasingly recognised that, in all tectonic contexts, the overarching control on magma pathways lies in the elastic stresses acting in the lithosphere (Anderson 1937a, 1939; Muller & Pollard 1977; Rubin 1995; Rivalta et al. 2015). Indeed, regardless of whether the rifting itself is driven by crustal stresses or by mantle flow and regardless of the mechanisms driving the production of melt in the mantle, once magma reaches the lithosphere its ascent pathways will be controlled by elastic stresses. In fact, magma transport through the lithosphere occurs mostly through diking, a form of hydraulic fracturing (e.g. Rubin 1995). As predominantly opening fractures, dikes tend to open roughly in the direction of least compression (e.g. Weertman 1971; Anderson 1937a, 1939; Nakamura 1977; Muller & Pollard 1977; Pollard 1987; Dahm 2000; Watanabe et al. 2002; Gudmundsson 2006, 2020).

Other authors, in approaches consistent with the physics of magma propagation, considered the role of stresses in influencing magma transport. Ellis & King (1991) suggested that flank volcanism in continental rifts could be explained by the dilational strain caused at the base of the footwall by faulting in a flexurally supported crust, which would favor upward magma propagation provided that melt is available in the lower crust. Maccaferri et al. (2014) proposed to include in the stress computations the unloading stresses induced by the formation of the rift excavation. They built a zero-order stress model by superposing a negative strip load (simulating the surface mass load missing in correspondence of the basin) to a uniform stretching of the lithosphere (Falvey 1974; Jarvis & McKenzie 1980; Le Pichon & Sibuet 1981). They then used a dike propagation code (Maccaferri et al. 2010, 2011) based on Dahm (2000) to simulate magma ascent in a 'gravitationally unloaded', extending rift. Their results show that when the unloading pressure dominates over the tectonic tension, the direction of least compression becomes vertical in a depth range under the basin, turning ascending dikes into subhorizontal magma bodies or forcing their way up to the rift flanks on oblique trajectories.

Here, we delve deeper in the Maccaferri et al. (2014) model to formulate a set of predictions that could be compared with current and future observations of rift-related volcanism. In particular, we test the ability of the model to predict the shifting through time of vent locations in rifts, along with the other overarching observations listed above, solely on the basis of evolving unloading and tectonic forces. To do so, we investigate how the progressive deepening of a rift basin re-orients the principal stresses in an elastic crust. We then simulate magma pathways using both simple principal stress direction principles and the more complex boundary element dike propagation code used by Maccaferri et al. (2014), which we have modified in order to account for two important effects that have been previously disregarded: the evolution trough time of the surface topography, and the stress interaction between successive dike intrusions.

First, we compile observations of the spatio-temporal evolution of volcanism and magmatism in rifting environments, in order to define common trends that can be compared with the predictions of our model. Second, we describe our model and its setup. Finally, we show the results of our simulations and comment on their implications with regards to magmatism in rifted areas.

2 OBSERVATIONS OF RIFT MAGMATISM

As an emblematic example of the shifting patterns introduced above, the Limagne Graben of the Massif Central Rift (MCR), France, experienced three main rifting-related magmatic events (Michon & Merle 2001) (Fig. 1). The first event preceded the formation of the rift basin and consisted of very scarce and scattered volcanism affecting a vast area comprising the future grabens and their surroundings. The second event immediately followed the formation of the graben and produced more than 200 monogenetic vents scattered in-rift to the North of the MCR, coinciding with the areas of pronounced crustal thinning; lastly, the major volcanic event mainly contributed to the formation of the Chaîne des Puys, the Monts Dore and Sancy stratovolcanoes and the Dèves basaltic shield, which are all located off-rift from the main graben; the more recent eruptions were also all confined to the outside of the basin. These latter major volcanic episodes were also associated with the uplift of the Massif Central, suggesting a common origin for uplift and volcanism. Michon & Merle (2001) proposed three different mechanisms for the generation of each of the three epochs of volcanism: lithospheric doming ahead of the incipient Alpine chain causing very low degrees of melting due to mantle decompression for the pre-rift phase, low degrees of melting associated with lithospheric thinning for the rift-related phase, and late thermal erosion of the base of the lithosphere above a mantle diapir for the major events. Michon & Merle (2001) also noticed that the development of the Eifel and the Ohře Eger rift in the Czeck Republic followed a nearly identical history (Bellon & Kopeckỳ 1977; Dudek & Eliáš 1984), with similar spatio-temporal and geochemical patterns.

Continental rifts are often associated with the presence of underplated material in the lower crust or upper mantle below the basin, usually occurring through the intrusion of sill-like magmatic sheets. This has been observed in a variety of extensional settings and rift zones, both modern and inactive ones (Thybo & Artemieva 2013). Birt et al. (1997) observed a strongly reflective lower crust directly below the Kenya Rift Graben, coherent with the presence of a high velocity underplated layer; Mackenzie et al. (2005) explained variations in seismic reflectivity in the lower crust beneath the Main Ethiopian Rift in terms of layered sills; Thybo & Nielsen (2009) attributed the high seismic velocity zone below the Baikal Rift, Russia to horizontal magmatic intrusions in the lower crust. Paleorifts like the North American Midcontinent Rift, USA and the Donbas Basin, Ukraine, also show evidence of large amounts of underplated material, as indicated by seismic models, constraints from gravity and anisotropy studies (Behrendt et al. 1990; Hinze et al. 1992; Meissner et al. 2006; Lyngsie et al. 2007).

If rifts progress towards later stages of deformation, volcanism starts to become progressively more confined to the axial portion of the basin, as part of the transition to oceanic spreading center. The Main Ethiopian Rift represents a unique environment where such transition can be currently investigated (Ebinger & Casey 2001; Corti 2012). The more recent Quaternary volcanics are in fact focused within the Wonji Fault Belt, which is located in the axial part of the graben, while many earlier Pliocene volcanoes have formed off-rift from the basin (Corti 2009).

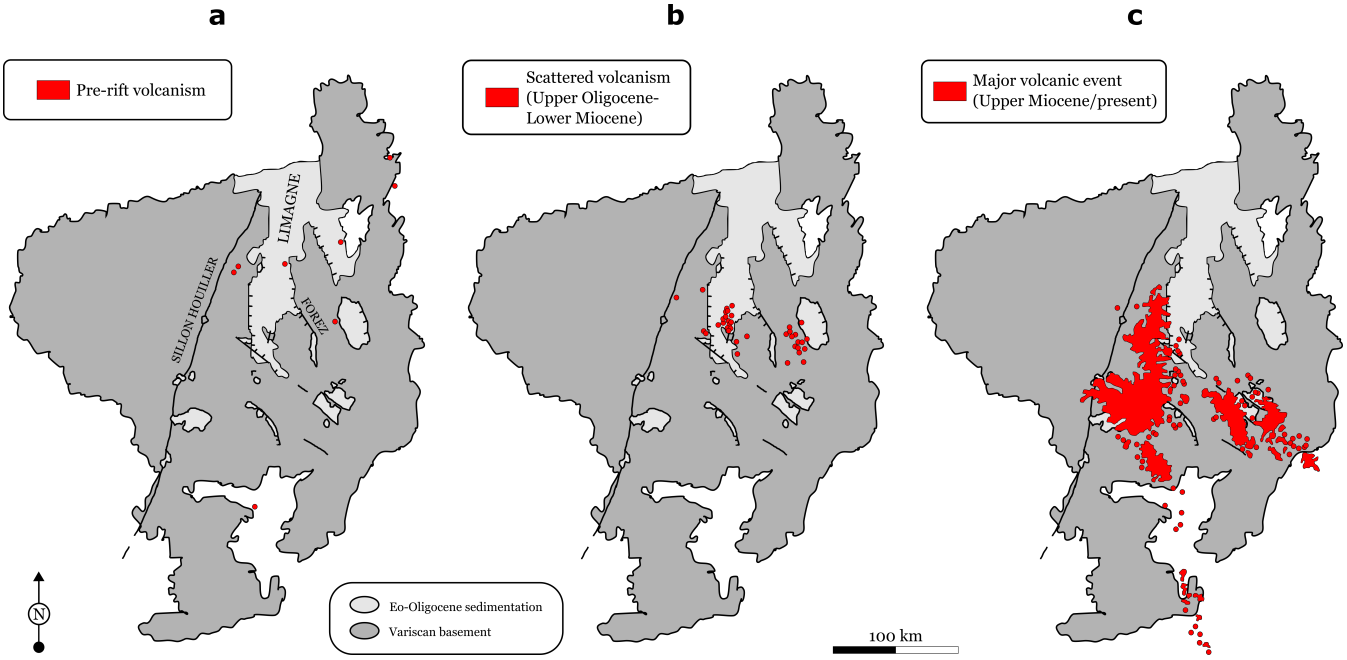

Figure 1. Spatio-temporal evolution of volcanism in the Massif Central Rift. The three panels represent the three different volcanic events. Modified from Michon & Merle (2001).

3 METHODS

Physics-based models of magma pathways may be broken down in two separate components (e.g. Neri et al. 2018; Rivalta et al. 2019):

(i) A model for the stress state of the earth's crust or lithosphere. The stress tensor is defined as a function of space and time, based on the the relevant stress-generating and stress-relieving mechanisms acting in the zone of interest.

(ii) A model for the trajectories followed by magma in a given stress field. Such models define a rule for magma propagation that takes as input the elastic stress field and a starting location for a magma batch, and return a magma pathway and an eruptive vent location should the pathway intersect the earth's surface.

3.1 Stress Model

3.1.1 Rift Deepening

We modeled the evolution of the state of stress of rift zones by reformulating the gravitational unloading model of Maccaferri et al. (2014) into a time-dependent problem. We adopted a 2-D plane strain assumption and modeled rift stresses by superposing a uniform strip-unloading of width W on the free surface of a half-space (e.g. Jaeger et al. 2009; Davis & Selvadurai 1996), simulating the creation of the rift excavation, to a uniform tectonic stretching of $\sigma_{tec} = 5$ MPa. The unloading pressure is $P = \rho g D$, where $\rho = 2900\,\mathrm{kg/m^3}$ is the crustal density, g the acceleration due to gravity and D the basin depth. The background state of stress is assumed to be lithostatic, rather than laterally confined as in Martel (2016).

By analytically comparing the intensity of the resulting principal vertical and horizontal stresses, Maccaferri et al. (2014) found that for $K = \frac{\pi}{2}\frac{\sigma_{tec}}{P} < 1$, the direction of least compression v_3 becomes vertical or sub-vertical over a depth interval under the basin spanned by the vertical coordinates z_1 and z_2:

$$z_1 = \frac{W}{2}\frac{1-\sqrt{1-K^2}}{K}, \quad z_2 = \frac{W}{2}\frac{1+\sqrt{1-K^2}}{K}. \tag{1}$$

This creates a stress barrier between z_1 and z_2 that deflects ascending dikes into sub-horizontal intrusions, forcing their way up to the rift flanks. Here, we considered a deepening basin as the rift evolves. For simplicity, we assumed that W remains constant throughout most of the rifting process and that the rift deepens at a constant deepening rate α, so that D evolves as

$$D = \alpha t. \tag{2}$$

The time dependent unloading pressure is therefore given by:

$$P(t) = \rho g D(t) = \rho g \alpha t. \tag{3}$$

Substituting eq. 3 in eqs 1 we obtained two equations for the time dependence of the stress barrier (Fig. 2):

$$z_1 = \frac{W}{\pi}\frac{\rho g \alpha t}{\sigma_{tec}}\left(1-\sqrt{1-\left(\frac{\pi}{2}\frac{\sigma_{tec}}{\rho g \alpha t}\right)^2}\right) \tag{4}$$

$$z_2 = \frac{W}{\pi}\frac{\rho g \alpha t}{\sigma_{tec}}\left(1+\sqrt{1-\left(\frac{\pi}{2}\frac{\sigma_{tec}}{\rho g \alpha t}\right)^2}\right). \tag{5}$$

At each deepening step, we computed the intensity and directions of the most compressive and least compressive stress axes, σ_1, σ_3, v_1 and v_3, respectively.

3.1.2 Rift Sedimentation

With the purpose of showing how additional time-varying contributions such as sedimentary loads may contribute to the stress field due to gravitational loading, we built on the stress field model described in Section 3.1.1 by adding further complexity due to the role of sedimentation. We conducted 20 sets of simulations for a $W = 100$ km wide full graben (Fig. 3). During the first 10 sets the

graben deepens from $D = 100$ m to $D = 1$ km at steps of 100 m each. This was obtained by applying a strip of gradually increasing unloading over the surface of an elastic half-space. The last 10 sets account for the role of sedimentation through the superposition of a strip loading increasing from a thickness of $T = 100$ m to $T = 800$ m, while the basin depth was kept fixed at $D = 1$ km. The effective unloading pressure at each set of simulations is thus given by

$$P_{eff}(t) = g(\rho D(t) - \rho_s T(t)) \quad (6)$$

where $\rho_s = 2700\,\mathrm{kg/m^3}$ is the density of the sediments.

3.2 Magma Pathways

3.2.1 Principal Stress Streamlines

The most basic model of magma trajectories was formulated by Anderson (1937a). According to the Anderson theory, faults and dikes have preferred orientations in the field according to their respective dislocation modes (Anderson 1951). Faults, being shear dislocations, tend to be oriented according to the optimal shearing direction, which is at an angle with respect to the directions of the minimum and maximum principal stresses, depending on friction (Anderson 1905). In contrast, dikes, needing to open and accommodate a volume, tend to intrude perpendicular to the least compressive principal stress axis, v_3 (Anderson 1939). Following this principle, first-order dike pathways can be calculated as streamlines perpendicular to v_3. This method has been used extensively in literature (e.g. Anderson 1937b; Muller & Pollard 1977; Pollard 1987; Chadwick & Dieterich 1995; Roman & Jaupart 2015; Oliva et al. 2022). We determined magma pathways and vent locations assuming that dikes propagate perpendicular to v_3, starting from a magma ponding zone as wide as the half-width of the graben located at the crust-mantle boundary $z_{\mathrm{Moho}} = 40$ km (Fig. 2).

3.2.2 Boundary Element Dike Trajectory Code

The methodology described in Section 3.2.1 does not account for the stress induced by the dike itself (that is for the effect of dike buoyancy); moreover, it does not return any information on whether the dike would propagate or become arrested somewhere along the trajectory. The trajectories computed through this method can be seen as 'potential trajectories' for dike propagation, showing the pathways that magma would follow, provided that dike buoyancy is large enough for the dike not to get arrested on its way along the trajectory. Numerical models that include fracture mechanics principles (Dahm 2000; Maccaferri et al. 2010; Davis et al. 2021) provide additional insights (Fig. 3). These models simulate self-propelled fracture propagation by considering dikes as pressurized fractures, filled with a buoyant, inviscid fluid, that move in any given stress field. The changing dike shape is modelled through the displacement discontinuity method (DDM) (Crouch et al. 1983), while the energetically-preferred magma trajectory is selected by identifying the pathway of maximum energy release rate (Griffith 1921). Here, we extended the code developed by Maccaferri et al. (2010, 2011) to account for the interaction between successive dike intrusions, following Kühn & Dahm (2008). At periodic timesteps, we used the stress field described in Section 3.1.2 as an input for for simulating multiple dike injections. (Fig. 3). Each injected dike has a magma density at atmospheric pressure of $2600\,\mathrm{kg/m^3}$. Less buoyant magmas would require more volume in order to propagate.

Throughout the simulations, we increased the number of injected dikes to represent intensified melting due to decompression of the asthenosphere, and we progressively decreased the depth of injection following the emplacement of progressively shallower crustal intrusions that can act as new locations of dike nucleation. The main parameters employed in the simulations are listed in Table 1, together with their values and units.

Table 1. Values of the parameters employed in the simulations

	Symbol	Value	Unit
Dike cross-sectional area	V	0.0075	$\mathrm{km^2}$
Initial dike length	l	5	km
Elementary dislocation length	l_0	0.1	km
Magma density	ρ_m	2600	$\mathrm{kg/m^3}$
Rock density	ρ	2900	$\mathrm{kg/m^3}$
Sedimentary layer density	ρ_s	2700	$\mathrm{kg/m^3}$
Magma bulk modulus	K	10	GPa
Rock rigidity	μ	20	GPa
Tectonic stress	σ_{tec}	5	MPa

4 RESULTS

4.1 Stress Field and Streamlines

As long as $t < t_c = \frac{\pi}{2}\frac{\sigma_{tec}}{\rho g \alpha}$, the basin is not deep enough for a stress barrier to form and the real parts of eqs 4 and 5 coincide (red patch in Fig. 2, panel **a**). As the basin deepens, the unloading pressure grows to eventually overcome the tectonic stresses, so that v_3 becomes vertical under the rift in a zone bounded by z_1 and z_2, creating a stress barrier. This happens for the critical depth $D_c = \frac{\pi\sigma_{tec}}{2\rho g}$, which is independent of rift width. In our case, this critical depth is about 280 m.

The stress barrier then broadens with time, with z_1 slowly approaching the surface while z_2 quickly descends to depth (Fig. 2, panel **a**). Also, for wider rifts, or as rifts get wider, the stress barrier forms at greater depths and grows faster. This is because z_1 and z_2 scale with rift width (eqs 4, 5). As a consequence, the barrier already extends beneath the Moho shortly after it has formed for rifts as wide as $W = 50$ km and forms in the lithospheric mantle, in this example, for $W > 85$ km.

We choose three snapshots from the time evolution of the barrier and analyze how magma pathways change from one D to the other (Fig. 2, panels **b** and **c**). As an example, we take the case of a $W = 25$ km wide full-graben (Fig. 2, panel **b**). When the basin is $D = 100$ m deep the tectonic tensile stresses dominate over the unloading pressure, causing the direction of least compression σ_3 to be roughly horizontal in the crust under the rift. As a consequence, dikes follow subvertical trajectories that result in scattered in-rift volcanism. As the basin deepens, a stress barrier is formed, so that for a $D = 400$ m deep basin the direction of σ_3 becomes vertical in a depth range under the rift axis. Ascending dikes are deflected towards the flanks, producing off-rift volcanism. This reproduces the shift from scattered in-rift vents to larger off-rift volcanoes occurring between the second and third stage of volcanism of the Limagne Graben (Section 2). The same result occurs when the rift is $D = 1$ km deep, with dikes reaching the flanks at greater distance from the basin, but in this case they are injected from inside the stress barrier. This already happens at shallower basin depths if wider rifts are considered (Fig. 2, panel **c**). After the nucleation of the stress barrier, dike trajectories become increasingly more tightly spaced as the rift deepens, reducing the distance between surface

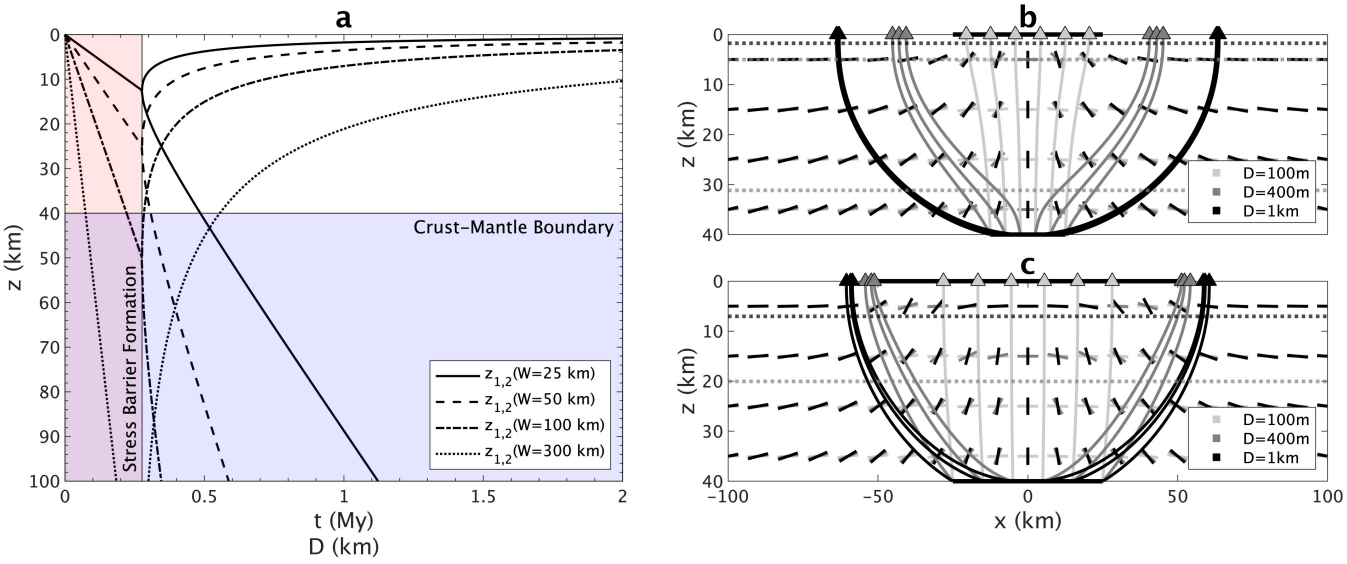

Figure 2. a: Evolution of the stress barrier: z_1 (upper branches) and z_2 (lower branches) for a full-graben deepening at a rate of $\alpha = 0.001$ m/y, plotted with respect to time for $W = 25$, 50, 100 and 300 km. Figure is patched in blue below the chosen depth of the Moho $z_{Moho} = 40$ km. Figure is patched in red up to the critical depth (or time) of stress barrier formation. **b-c**: Directions of least compression (short segments), dike trajectories (curved lines) and surface arrivals (triangles) in a $W = 25$ km (**a**) and a $W = 100$ km (**b**) wide full-graben for $D = 100$ m (light gray), $D = 400$ m (dark gray) and $D = 1$ km (black). A uniform horizontal tensional stress $\sigma_{tec} = 5$ MPa is superimposed to the unloading stresses. Horizontal lines represent the upper and lower limits of the stress barrier. Black bold segments at $z = 0$ km and $z = 40$ km represent the extent of the rift and the magma ponding zone, respectively.

arrivals and promoting the formation of a few large polygenetic volcanic edifices.

4.2 Magmatic Dike Simulations

From our simulations, we identify four main stages in the development of rift-related volcanism (Fig. 3). At first, the rift is not deep enough for a stress barrier to be formed, so that dikes ascend sub-vertically towards the surface of the basin (Fig. 3, panel **a**). Dike eruptions are scattered across the rift depression during this first stage. As the rift deepens a stress barrier is formed and dikes are deflected towards the flanks of the depression, resulting in a shift to off-rift eruptions. These two stages were already predicted by the analytical results shown in Section 4.1. Dikes simulations, however, reveal that if the stress barrier extends beyond the dike injection depth (the conditions are $D > \pi\sigma_{\rm tec}/(2\rho g) \approx 280\,$m, and $z_{\rm inj} > z_1$), dikes injected close to the rift axis may lack the buoyancy needed to ascend, so that they may get trapped as horizontal sill-like structures in the lower crust (Fig. 3, panel **b**). These horizontal intrusions can in turn collect melt supplied by further injections from below and serve as magma ponding zones from where subsequent dikes are nucleated. This way, progressively shallower horizontal intrusions form, promoting the stacking of the sills under the rift (Fig. 3, panel **c**), causing $z_{\rm inj}$ to approach z_1. This explains the ubiquitous presence of sill-like lower crustal intrusions in rifting environments (Section 2). At this point, two scenarios are possible. If the sedimentation rate $\alpha_{\rm T}$ meets the condition $\alpha_{\rm T} > \alpha\rho/(\rho_s)$, the loading rate due to sedimentation dominates over the unloading rate due to rift deepening. Hence, the loading due to the accumulation of sediments progressively compensates the unloading induced by the excavation of the rift, causing z_1 to deepen and eventually overcome z_{inj}. The following dikes are injected and propagate from above a deep barrier, implying slightly diverging trajectories and resulting in monogenetic in-rift volcanoes. In contrast, if $\alpha_{\rm T} < \alpha\rho/(\rho_s)$, the sediment loading rate is dominated by the unloading rate due to rift deepening. Thus, sill injections progressively shallow, leading to a shallowing of z_{inj}, until eventually z_{inj} approaches a more slowly shallowing z_1. When z_{inj} coincides with z_1, the shallowest possible sill is created at a depth of about z_1. Dikes injected from the sill at the top of the pile erupt inside the rift basin. However, unlike for the previous deep injection cases, the nucleation depth, depending on the rift parameters, may now be shallow. This results in a later stage where volcanism focuses in the axial part of the rift (Fig. 3, panel **d**). A dike nucleating from this shallow depth is expected to be oriented vertically (see orientation of principal stresses above z_1 in Fig. 2, panel **b**) and propagate laterally along the rift axis. Thus, stress-driven dikes in this phase may dislocate at once the entire 'intact' layer of crust above the stacked sills and create the conditions for a more focused crustal splitting, representing a shift from continental rifting to incipient oceanic spreading (e.g. Ebinger et al. 2010).

5 DISCUSSION AND CONCLUSIONS

The main limitation of our model is that it does not simulate some rifting-related processes that are usually accounted for in geodynamical models, such as melting and rheological layering. Despite these simplifications, our first order simulations of magma propagation in an evolving rift are able to highlight the main control exerted by crustal stress changes - and their link with the evolving topography - on the propagation paths followed by magmatic intrusions. Combining our model approach with sophisticated geodynamical models would allow for further constraining the dike simulations (for instance in terms of melt volumes and magma properties), and provide improved crustal stress estimates.

In our model, melt is assumed to be available from the very beginning of the rifting process. This is true only for plume-related rifts, while in passive rifts a minimum graben depth would be required for melting to start. Inhibited melt production during rift ini-

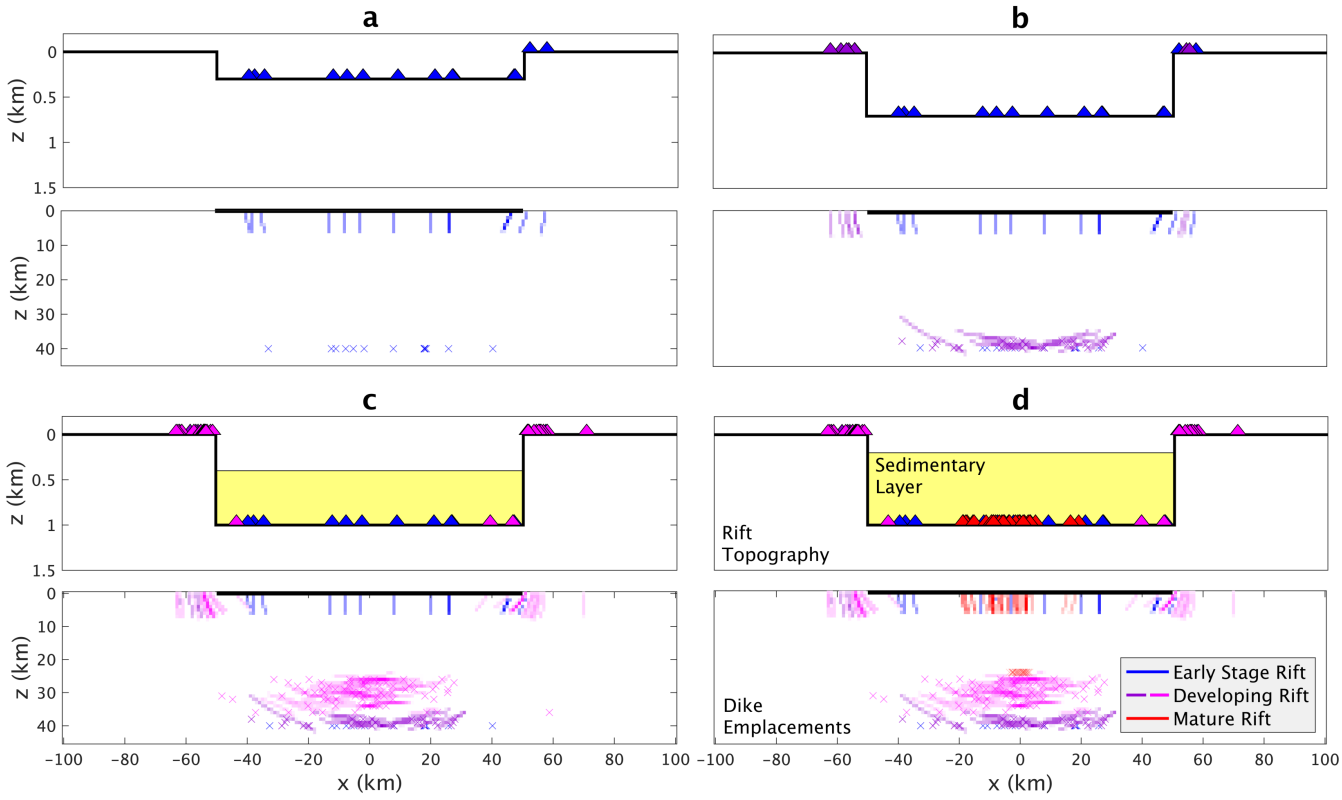

Figure 3. a-d: The four stages of rift-related volcanism identified in our simulations. **a**: Early scattered in-rift volcanism. **b**: Off-rift volcanism and sill formation. **c**: Sill stacking and off-rift volcanism. **d**: Late axial in-rift volcanism. *Upper panels*: Bold line represents rift topography. Sedimentary layer is patched in yellow. Colored triangles mark the locations of surface dike arrivals. *Lower panels*: Density plots of dike emplacements. Colored crosses indicate the coordinates at which dikes are injected.

tiation could result in preventing early in-rift volcanism, essentially skipping or reducing the duration of the first stage of our simulations. The overall pattern of magmatism, however, together with the relative timing of the different stages, would still be preserved.

Although a visco-elastic rheology could better approximate the behaviour of the lower crust, a full elastic assumption has been employed in this work. Seismic evidence shows that a strong mid-lower crust is present below young rifts (Déverchère et al. 2001; Craig et al. 2011). This is also proven by topographies of wavelengths up to hundreds of kms lasting tens of millions of years, that imply the existence of a thick layer behaving rigidly over the same timespan (Turcotte 1979). Moreover, dike propagation can also occur in a visco-elastic material, provided that the viscosity contrast between the rock and the magma is larger than $10^{11} - 10^{14}$, which is generally true for basaltic magmas and low-viscosity rhyolitic magmas (Rubin 1993). In fact, magmatic underplating under continental rifts often occurs through the emplacement of sills (Thybo & Nielsen 2009; Thybo & Artemieva 2013), meaning that magma is still able to move by hydraulic fracturing in the lower crust.

Prolonged extension in rifts can result in the shallowing of the Moho due to crustal thinning (Ruppel 1995), the emplacement of sill-like horizontal magma bodies in the lower crust (Thybo & Nielsen 2009) or a combination thereof (Thybo & Artemieva 2013). These crustal intrusions appear as high seismic velocity, high reflectivity structures in seismic studies (Thybo & Nielsen 2009; Thybo & Artemieva 2013). In our simulations the evolving geometry of the basin controls the emplacement of sills below the rift, which in turn is expected to control the amount of Moho uplift required to obtain isostatic equilibrium.

In conclusion, we propose that the temporal evolution of crustal stresses in rift zones, as a result of the progressive development of the gravitational unloading of the basin and tectonic stretching, may exert a top-down control on the evolution of magma pathways and surface vent distribution, ultimately producing the observed patterns of magmatism. While our current model does not address the petrological aspects of rift volcanism, we expect that the different stages envisioned by our model, corresponding to different depths and timescales of stagnation of magma in the crust, should leave a detectable signature on the petrology of the erupted lavas and released gases, which can be further scrutinized in future studies on the subject.

In spite of its simplifications, our model captures the main features of how the distribution of volcanism shifts over time while the rift matures. This implies that most of these common features may solely depend on the top-down/remote driving factors considered in our model, that is gravitational stresses due to an evolving graben topography and tectonic extension, and largely disentangled from bottom-up factors such as whether melt is generated by active vs. passive rifting.

Once applied more closely to individual rifts, the model presented in this work may also help shed light on the possible mechanisms underlying rift initiation.

ACKNOWLEDGMENTS

This research was funded by the German Research Foundation (DFG), Grant 634756, RI 2782/2.

DATA AVAILABILITY

The Fortran90 code used for the numerical dike simulations and the instructions on how to compile and run the code will be available via Zenodo repository upon publication. All the data used as input for the simulations are attached as supporting information.

REFERENCES

Acocella, V., 2021. *Volcano-Tectonic Processes*, Springer Nature.

Anderson, E., 1937a. Cone-sheets and ring-dykes: the dynamical explanation, *Bulletin Volcanologique*, **1**(1), 35–40.

Anderson, E., 1939. Xvii.—the dynamics of sheet intrusion, *Proceedings of the Royal Society of Edinburgh*, **58**, 242–251.

Anderson, E., 1951. *The Dynamics of Faulting and Dyke Formation*, Oliver and Boyd, Edinburgh.

Anderson, E. M., 1905. The dynamics of faulting, *Transactions of the Edinburgh Geological Society*, **8**(3), 387–402.

Anderson, E. M., 1937b. Ix.—the dynamics of the formation of cone-sheets, ring-dykes, and caldron-subsidences, *Proceedings of the Royal Society of Edinburgh*, **56**, 128–157.

Behrendt, J. C., Hutchinson, D., Lee, M., Thornber, C., Trehu, A., Cannon, W., & Green, A., 1990. Glimpce seismic reflection evidence of deep-crustal and upper-mantle intrusions and magmatic underplating associated with the midcontinent rift system of north america, *Tectonophysics*, **173**(1-4), 595–615.

Bellon, H. & Kopeckỳ, L., 1977. Spectres d'ages radiométriques du volcanisme du rift du massif bohémien.–5eme réunion ann, *Sci. Terre, Rennes, Soc. Géol. Fr. éd*, **57**.

Birt, C., Maguire, P., Khan, M., Thybo, H., Keller, G. R., & Patel, J., 1997. The influence of pre-existing structures on the evolution of the southern kenya rift valley—evidence from seismic and gravity studies, *Tectonophysics*, **278**(1-4), 211–242.

Bosworth, W., 1987. Off-axis volcanism in the gregory rift, east africa: Implications for models of continental rifting, *Geology*, **15**(5), 397–400.

Bott, M., 2006. Mechanisms of rifting: geodynamic modeling of continental rift systems, in *Developments in Geotectonics*, vol. 25, pp. 27–43, Elsevier.

Chadwick, W. & Dieterich, J., 1995. Mechanical modeling of circumferential and radial dike intrusion on galapagos volcanoes, *Journal of Volcanology and Geothermal Research*, **66**(1-4), 37–52.

Condie, K. C., 2013. *Plate tectonics & crustal evolution*, Elsevier.

Corti, G., 2009. Continental rift evolution: from rift initiation to incipient break-up in the main ethiopian rift, east africa, *Earth-Science Reviews*, **96**(1-2), 1–53.

Corti, G., 2012. Evolution and characteristics of continental rifting: Analog modeling-inspired view and comparison with examples from the east african rift system, *Tectonophysics*, **522**, 1–33.

Corti, G., Bonini, M., Sokoutis, D., Innocenti, F., Manetti, P., Cloetingh, S., & Mulugeta, G., 2004. Continental rift architecture and patterns of magma migration: A dynamic analysis based on centrifuge models, *Tectonics*, **23**(2).

Craig, T., Jackson, J., Priestley, K., & McKenzie, D., 2011. Earthquake distribution patterns in africa: their relationship to variations in lithospheric and geological structure, and their rheological implications, *Geophysical Journal International*, **185**(1), 403–434.

Crouch, S. L., Starfield, A. M., & Rizzo, F., 1983. *Boundary element methods in solid mechanics*, George Allen and Unwin.

Dahm, T., 2000. Numerical simulations of the propagation path and the arrest of fluid-filled fractures in the earth, *Geophysical Journal International*, **141**(3), 623–638.

Davis, R. & Selvadurai, A., 1996. *Elasticity and geomechanics*, Cambridge University Press.

Davis, T., Bagnardi, M., Lundgren, P., & Rivalta, E., 2021. Extreme curvature of shallow magma pathways controlled by competing stresses: insights from the 2018 sierra negra eruption, *Geophysical Research Letters*, **48**(13), e2021GL093038.

Déverchère, J., Petit, C., Gileva, N., Radziminovitch, N., Melnikova, V., & San'Kov, V., 2001. Depth distribution of earthquakes in the baikal rift system and its implications for the rheology of the lithosphere, *Geophysical Journal International*, **146**(3), 714–730.

Dudek, A. & Eliáš, M., 1984. Magmatic history, *Geological history of the territory of the Czech Soc. Republic. Academia Publishing, House of Czech Akademie of Sciences*, pp. 229–262.

Ebinger, C. & Casey, M., 2001. Continental breakup in magmatic provinces: An ethiopian example, *Geology*, **29**(6), 527–530.

Ebinger, C., Ayele, A., Keir, D., Rowland, J., Yirgu, G., Wright, T., Belachew, M., & Hamling, I., 2010. Length and timescales of rift faulting and magma intrusion: The afar rifting cycle from 2005 to present, *Annual Review of Earth and Planetary Sciences*, **38**(1), 439–466.

Ellis, M. & King, G., 1991. Structural control of flank volcanism in continental rifts, *Science*, **254**(5033), 839–842.

Falvey, D. A., 1974. The development of continental margins in plate tectonic theory, *The APPEA Journal*, **14**(1), 95–106.

Fitton, J. G., 1983. Active versus passive continental rifting: evidence from the west african rift system, *Tectonophysics*, **94**(1-4), 473–481.

Griffith, A. A., 1921. Vi. the phenomena of rupture and flow in solids, *Philosophical transactions of the royal society of london. Series A, containing papers of a mathematical or physical character*, **221**(582-593), 163–198.

Gudmundsson, A., 2006. How local stresses control magma-chamber ruptures, dyke injections, and eruptions in composite volcanoes, *Earth-science reviews*, **79**(1-2), 1–31.

Gudmundsson, A., 2020. *Volcanotectonics: Understanding the structure, deformation and dynamics of volcanoes*, Cambridge University Press.

Hinze, W. J., Allen, D. J., Fox, A. J., Sunwood, D., Woelk, T., & Green, A. G., 1992. Geophysical investigations and crustal structure of the north american midcontinent rift system, *Tectonophysics*, **213**(1-2), 17–32.

Ivanov, A. V., Demonterova, E. I., He, H., Perepelov, A. B., Travin, A. V., & Lebedev, V. A., 2015. Volcanism in the baikal rift: 40 years of active-versus-passive model discussion, *Earth-Science Reviews*, **148**, 18–43.

Jaeger, J. C., Cook, N. G., & Zimmerman, R., 2009. *Fundamentals of rock mechanics*, John Wiley & Sons.

Jarvis, G. T. & McKenzie, D. P., 1980. Sedimentary basin formation with finite extension rates, *Earth and Planetary science letters*, **48**(1), 42–52.

Kiselev, A., 1987. Volcanism of the baikal rift zone, *Tectonophysics*, **143**(1-3), 235–244.

Kühn, D. & Dahm, T., 2008. Numerical modelling of dyke interaction and its influence on oceanic crust formation, *Tectonophysics*, **447**(1-4), 53–65.

Le Pichon, X. & Sibuet, J.-C., 1981. Passive margins: a model of formation, *Journal of Geophysical Research: Solid Earth*, **86**(B5), 3708–3720.

Lesne, O., Calais, E., & Deverchere, J., 1998. Finite element modelling of crustal deformation in the baikal rift zone: new insights into the active–passive rifting debate, *Tectonophysics*, **289**(4), 327–340.

Logatchev, N. & Florensov, N., 1978. The baikal system of rift valleys, *Tectonophysics*, **45**(1), 1–13.

Lyngsie, S. B., Thybo, H., & Lang, R., 2007. Rifting and lower crustal reflectivity: A case study of the intracratonic dniepr-donets rift zone, ukraine, *Journal of Geophysical Research: Solid Earth*, **112**(B12).

Maccaferri, F., Bonafede, M., & Rivalta, E., 2010. A numerical model of dyke propagation in layered elastic media, *Geophysical Journal International*, **180**(3), 1107–1123.

Maccaferri, F., Bonafede, M., & Rivalta, E., 2011. A quantitative study of the mechanisms governing dike propagation, dike arrest and sill formation, *Journal of Volcanology and Geothermal Research*, **208**(1-2), 39–50.

Maccaferri, F., Rivalta, E., Keir, D., & Acocella, V., 2014. Off-rift volcanism in rift zones determined by crustal unloading, *Nature Geoscience*, **7**(4), 297–300.

Mackenzie, G., Thybo, H., & Maguire, P., 2005. Crustal velocity structure across the main ethiopian rift: results from two-dimensional wide-angle seismic modelling, *Geophysical Journal International*, **162**(3), 994–1006.

Martel, S. J., 2016. Effects of small-amplitude periodic topography on combined stresses due to gravity and tectonics, *International Journal of Rock Mechanics and Mining Sciences*, **89**, 1–13.

Meissner, R., Rabbel, W., & Kern, H., 2006. Seismic lamination and anisotropy of the lower continental crust, *Tectonophysics*, **416**(1-4), 81–99.

Michon, L. & Merle, O., 2001. The evolution of the massif central rift; spatio-temporal distribution of the volcanism, *Bulletin de la Société géologique de France*, **172**(2), 201–211.

Morton, W. H., Rex, D., Mitchell, J., & Mohr, P., 1979. Riftward younging of volcanic units in the addis ababa region, ethiopian rift valley, *Nature*, **280**(5720), 284–288.

Muller, O. H. & Pollard, D. D., 1977. The stress state near spanish peaks, colorado determined from a dike pattern, *Pure and Applied Geophysics*, **115**(1), 69–86.

Nakamura, K., 1977. Volcanoes as possible indicators of tectonic stress orientation—principle and proposal, *Journal of Volcanology and Geothermal Research*, **2**(1), 1–16.

Neri, M., Rivalta, E., Maccaferri, F., Acocella, V., & Cirrincione, R., 2018. Etnean and hyblean volcanism shifted away from the malta escarpment by crustal stresses, *Earth and Planetary Science Letters*, **486**, 15–22.

Oliva, S. J., Ebinger, C. J., Rivalta, E., Williams, C. A., Wauthier, C., & Currie, C. A., 2022. State of stress and stress rotations: Quantifying the role of surface topography and subsurface density contrasts in magmatic rift zones (eastern rift, africa), *Earth and Planetary Science Letters*, **584**, 117478.

Pollard, D. D., 1987. Elementary fracture mechanics applied to the structural interpretation of dykes, in *Mafic dyke swarms*, vol. 34, pp. 5–24, Geological Association of Canada.

Rivalta, E., Taisne, B., Bunger, A., & Katz, R., 2015. A review of mechanical models of dike propagation: Schools of thought, results and future directions, *Tectonophysics*, **638**, 1–42.

Rivalta, E., Corbi, F., Passarelli, L., Acocella, V., Davis, T., & Di Vito, M. A., 2019. Stress inversions to forecast magma pathways and eruptive vent location, *Science advances*, **5**(7), eaau9784.

Roman, A. M. & Jaupart, C. P., 2015. Post-emplacement behaviour of magma reservoirs, in *AGU Fall Meeting Abstracts*, vol. 2015, pp. V42B–03.

Rubin, A. M., 1993. Dikes vs. diapirs in viscoelastic rock, *Earth and Planetary Science Letters*, **117**(3-4), 653–670.

Rubin, A. M., 1995. Propagation of magma-filled cracks, *Annual Review of Earth and Planetary Sciences*, **23**(1), 287–336.

Ruppel, C., 1995. Extensional processes in continental lithosphere, *Journal of Geophysical Research: Solid Earth*, **100**(B12), 24187–24215.

Thybo, H. & Artemieva, I., 2013. Moho and magmatic underplating in continental lithosphere, *Tectonophysics*, **609**, 605–619.

Thybo, H. & Nielsen, C., 2009. Magma-compensated crustal thinning in continental rift zones, *Nature*, **457**(7231), 873–876.

Turcotte, D. L., 1979. Flexure, in *Advances in geophysics*, vol. 21, pp. 51–86, Elsevier.

Watanabe, T., Masuyama, T., Nagaoka, K., & Tahara, T., 2002. Analog experiments on magma-filled cracks: Competition between external stresses and internal pressure, *Earth, planets and space*, **54**(12), e1247–e1261.

Weertman, J., 1971. Theory of water-filled crevasses in glaciers applied to vertical magma transport beneath oceanic ridges, *Journal of Geophysical Research*, **76**(5), 1171–1183.

White, R., 1992. Magmatism during and after continental break-up, *Geological Society, London, Special Publications*, **68**(1), 1–16.

Williams, L., 1982. Physical aspects of magmatism in continental rifts, *Continental and oceanic rifts*, **8**, 193–222.

Ziv, A., Rubin, A. M., & Agnon, A., 2000. Stability of dike intrusion along preexisting fractures, *Journal of Geophysical Research: Solid Earth*, **105**(B3), 5947–5961.